

Side Fenestrations Provide an “Anchor” for a Stable Binding of A1899 to the Pore of TASK-1 Potassium Channels

David Ramírez,^{†,‡} Bárbara Arévalo,[†] Gonzalo Martínez,[†] Susanne Rinné,[§] Francisco V. Sepúlveda,^{||} Niels Decher,^{*,§} and Wendy González^{*,†,‡}

[†]Centro de Bioinformática y Simulación Molecular, Universidad de Talca, 1 poniente No. 1141, 3460000 Talca, Chile

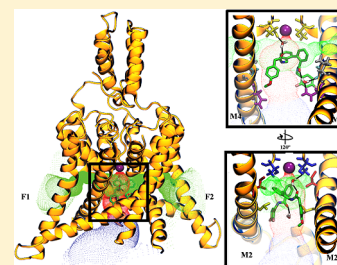
[‡]Instituto de Ciencias Biomédicas, Universidad Autónoma de Chile, 5 Poniente No. 1670, 3460000 Talca, Chile

[§]Institute for Physiology and Pathophysiology, Vegetative Physiology Group, University of Marburg, 35037 Marburg, Germany

^{||}Centro de Estudios Científicos (CECs), Arturo Prat 514, 5110000 Valdivia, Chile

Supporting Information

ABSTRACT: A1899 is a potent and selective inhibitor of the two-pore domain potassium (K_{2P}) channel TASK-1. It was previously reported that A1899 acts as an open-channel blocker and binds to residues of the P1 and P2 regions, the M2 and M4 segments, and the halothane response element. The recently described crystal structures of K_{2P} channels together with the newly identified side fenestrations indicate that residues relevant for TASK-1 inhibition are not purely facing the central cavity as initially proposed. Accordingly, the TASK-1 binding site and the mechanism of inhibition might need a re-evaluation. We have used TASK-1 homology models based on recently crystallized K_{2P} channels and molecular dynamics simulation to demonstrate that the highly potent TASK-1 blocker A1899 requires binding to residues located in the side fenestrations. Unexpectedly, most of the previously described residues that interfere with TASK-1 blockade by A1899 project their side chains toward the fenestration lumina, underlining the relevance of these structures for drug binding in K_{2P} channels. Despite its hydrophobicity, A1899 does not seem to use the fenestrations to gain access to the central cavity from the lipid bilayer. In contrast, binding of A1899 to residues of the side fenestrations might provide a physical “anchor”, reflecting an energetically favorable binding mode that after pore occlusion stabilizes the closed state of the channels.



KEYWORDS: TASK-1, ion channels, A1899, molecular docking, molecular dynamics, drug–protein interaction

INTRODUCTION

Two-pore domain potassium (K_{2P}) channels are widely expressed in the central nervous system and the cardiovascular, genitourinary, and gastrointestinal systems.¹ The mammalian K_{2P} channel family consists of 15 family members divided into six subfamilies based on sequence similarity and their functional hallmarks.² They are crucial for setting the resting membrane potential, regulation of excitability, ion transport, sensory transduction, metabolic regulation, and neuroprotection, just to name some (patho)physiological processes and therapeutical potentials.³

The TASK subgroup includes three members: TASK-1,⁴ TASK-3,⁵ and TASK-5.⁶ Functional K_{2P} channels form dimers, and each subunit has two pore-forming loops (P1, P2), four transmembrane domains (M1–M4), and an extended extracellular loop between M1 and P1.⁷ The crystallized structures of K_{2P} channels TWIK-1,⁸ TRAAK,^{9,10} TREK-1 (PDB: 4TWK), and TREK-2¹¹ reveal differences giving insights into distinctive gating and ion permeation properties. Near the membrane center, the M2 transmembrane segment is kinked by approximately 20°. This twist generates in each subunit a fenestration: open lateral passages connecting the pore with the lipid bilayer inner leaflet.¹² Recently it has been hypothesized that opening or closing of the fenestrations in response to

bilayer inner leaflet deformation determines the gating of TRAAK channel by allowing lipids to penetrate into the inner cavity and interfering with ion permeation. The conductive and nonconductive conformations of TRAAK channels would therefore be associated with the closed and open fenestration state, respectively.¹³ However, one should mention that this view of TRAAK gating mechanism is not shared by a contemporary structural study,¹⁴ or by an experimental work pointing to a selectivity filter opening and closing as the sole mechanism of K_{2P} channel gating.^{15–17} Nevertheless, the intramembrane fenestrations appear to be important in the interaction of lipids and hydrophobic molecules with K_{2P} channels. This is supported by the work of Dong et al., which describes how lipids and other hydrophobic molecules such as Prozac interact with the TREK-2 fenestrations.¹¹ These side cavities of K_{2P} channels are, therefore, potentially mechanistic “active sites” and/or pathways which can warrant blockers access to their binding sites.

Received: January 6, 2017

Revised: April 26, 2017

Accepted: May 11, 2017

Published: May 11, 2017

K_{2P} channels have been associated with several human pathophysiological processes and can also provide novel therapeutic options: for instance TASK-1 is an important modulator of multiple sclerosis¹⁸ and modulates T cell effector function.¹⁹ These channels are blocked by a variety of compounds and molecules, such as bupivacaine,²⁰ Zn²⁺,²¹ doxapram,²² loratadine, mevastatin, mibefradil, and octoclothe-pin,²³ and also by congeneric series such as THPP-derived compounds²⁴ and bis-amide derived compounds.²⁵ The highly potent TASK-1 blocker A1899, originally designed as a Kv1.5 channel blocker but with a strong preference for TASK-1 channels,²⁶ blocks TASK-1 in the low nanomolar range.²⁷ The blockade is selective for TASK-1 as the closely related TASK-3 channel is inhibited with only a tenth of the potency. It was previously reported that A1899 acts as an open-channel blocker and binds to residues at P1 and P2 regions, M2 and M4 segments, and the halothane response element.²⁷ The presence of side fenestrations within the crystallized structures of K_{2P} channels might redefine the drug binding site of TASK channels, initially proposed at the wall of the central cavity. In the same way side fenestrations might represent a route for A1899 to access its binding site. In this study, we describe the binding mechanism of A1899 to TASK-1 by using several computational techniques as well as experimental electrophysiological measurements. Our results show that A1899 binds to the central cavity and causes physical pore occlusion. They are in agreement with those reported by Chokshi et al. where they found that compounds A1899, PK-THPP, and doxapram inhibit TASK-3 channels by binding at a common site in the central cavity.²⁸ However, most of the residues relevant for TASK-1 inhibition by A1899 face into the side fenestrations, nevertheless A1899 does not appear to travel from the membrane through the fenestrations to reach the binding site in the central cavity.

EXPERIMENTAL SECTION

Scheme 1 summarizes the major steps followed in the present work to formulate a hypothesis about the configuration of A1899 inhibitor binding site in TASK-1 channel, which will be presented in more detail within the Experimental Section.

TASK-1 Homology Modeling. Since the structure of human TASK-1 channel has not yet been solved, we built four homology models for TASK-1 (UniProtKB accession number: O14649) using as template the crystal structures of TRAAK channel (PDBs: 419W, 3UM7), TREK-2 (PDB: 4BWS), and TWIK-1 (PDB: 3UKM), according to the multiple sequence alignment published by Brohawn et al.⁹ (Figure S2 in the Supplementary Data of ref 9). The rationale for using multiple structures as templates for the TASK-1 homology models was a need to study the interactions between A1899 and the fenestrations in open and closed conformations. The four homology models (PDB files provided in the [Supporting Information](#)) were named according to the template and the fenestration state of the structures used ([Table 1](#)). The models are named T1treCC (TASK-1 from TREK-2 in closed–closed fenestration state); T1twiOO (TASK-1 from TWIK-1 in open–open fenestration state), T1trCO (TASK-1 from TRAAK in closed–open fenestration state), and T1trOO (TASK-1 from TRAAK in open–open fenestration state) ([Figure S1](#)). The amino acids that were included in each TASK-1 model are as follows: T1treCC, Arg³ to Asn²⁵⁰; T1twiOO, Lys² to Ala²⁵¹; T1trCO, Arg³ to Met²⁴⁹; and T1trOO, Met¹ to Asp²⁵³. TASK-1 homology models were built

Scheme 1. Flow Chart Summarizing the Steps Followed in the Present Work To Formulate a Hypothesis about the Configuration of A1899 Inhibitor Binding Site in TASK-1 Channel

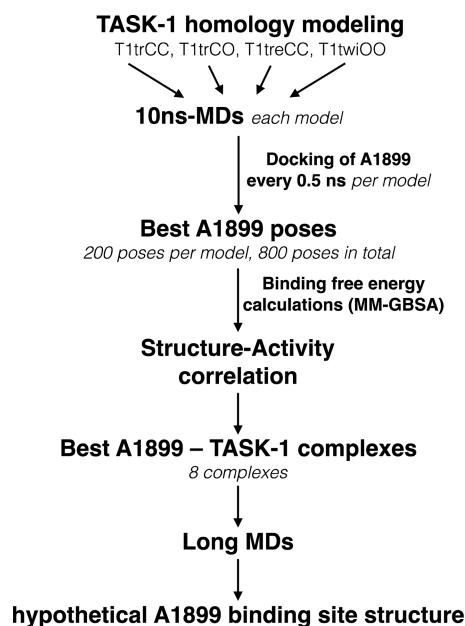


Table 1. Nomenclature of the TASK-1 Homology Models

template	TASK-1 homology model name
TREK-2 (PDB: 4BWS)	T1treCC
TWIK-1 (PDB: 3UMK)	T1twiOO
TRAAK (PDB: 419W)	T1trCO
TRAAK (PDB: 3UM7)	T1trOO

and optimized using ICM software.²⁹ Models were built as monomers and assembled as dimers using the STAMP algorithm³⁰ implemented in VMD program;³¹ then they were validated using PROCHECK.³² Two K⁺ ions were associated with the models in positions S2 and S4 of the selectivity filter and two water molecules at sites S1 and S3. Schrödinger Master version 9.2 software³³ interface was used to add hydrogen atoms by assigning the bonds and charges to the homology models.

The models were embedded into a pre-equilibrated phosphatidyl oleoylphosphatidylcholine (POPC) bilayer in a periodic boundary condition box with pre-equilibrated simple point charge (SPC) water molecules. The OPLS-2005 force field^{34,35} was used to add charges and atom types to the TASK-1 homology models, ions, lipids, and waters. Each system was subjected to a conjugate gradient energy minimization and 10 ns molecular dynamics simulation (MDs) in Desmond v3.0 program.^{33,36} A restriction was applied to the protein backbone atoms and the K⁺ ions at the selectivity filter using a spring constant force of 0.5 kcal mol⁻¹ Å⁻².

HOLE Radius Profiles. To determine the dimensions of the fenestrations and the pore, the algorithm HOLE was used.³⁷ For each MDs, one snapshot each 0.5 ns was taken. A total of 80 structures (20 per model) were collected from the TASK-1 homology model MDs to perform HOLE and further analyses.

A1899 Modeling. The TASK-1 blocker A1899 ([Figure S2A](#)) was sketched with the GaussView software³⁸ and optimized with the Gaussian09 software³⁹ by using the hf/3-

21g *ab initio* calculations⁴⁰ to obtain the equilibrium geometry, the geometrical parameters, and the potential energy surfaces. Later, A1899 was processed using LigPrep³³ with the force field OPLS_2005.⁴¹ The charges were maintained during the parametrization process before docking and molecular dynamics simulations.

Molecular Docking. To find the best A1899 pose interacting with TASK-1 models, and considering the flexibility of the receptor, we performed several molecular dockings in the structures collected every 0.5 ns (20 structures) from the 10 ns MDs of all homology models using the software Glide v5.7^{33,42} and the standard precision (SP) scoring function, obtaining 10 poses per docking simulation. The incorporation of conformational rearrangements of the receptor binding pocket into predictions of the ligand binding pose was critical for improving docking results.^{43,44} The ligand-binding site was defined by the residues forming the experimentally determined binding site of A1899 in TASK-1.²⁷ The center of the grid box was focused into the residues Thr⁹² and Thr¹⁹⁸ at the bottom of the selectivity filter. The molecular docking simulations were carried out with the outer box edge of the grid setting as 30 Å. The generated grid information for each receptor is given in Table S1 and in Figure S3. We obtained a total of 200 poses (10 poses for each frame, 20 frames for each model) per model.

Rescore of Docking Poses Using MM-GBSA. To overcome the different limitations and challenges of molecular docking method such as the prediction of correct binding modes and the accurate estimation of the corresponding binding affinity (prediction performed by the scoring function^{45,46}), the 200 A1899 poses per model obtained previously were postprocessed by using the molecular mechanics generalized Born surface area (MM-GBSA) method implemented in Prime software.³³ This method combines molecular mechanics energy and implicit solvation models,⁴⁷ and it has been employed to rescore docking solutions, resulting in the prediction of better binding modes compared with the results obtained with the docking scoring functions alone.^{48–51}

In MM-GBSA, the binding free energy between the ligand (A1899) and the receptor (TASK-1 channel) to form a complex is calculated as

$$\Delta G_{\text{bind}} = \Delta H - T\Delta S \approx \Delta E_{\text{MM}} + \Delta G_{\text{sol}} - T\Delta S \quad (1)$$

where $\Delta E_{\text{MM}} = \Delta E_{\text{internal}} + \Delta E_{\text{vdw}}$ and $\Delta G_{\text{sol}} = \Delta G_{\text{PB/GB}} + \Delta G_{\text{SA}}$. ΔE_{MM} , ΔG_{sol} and $T\Delta S$ are the changes in the molecular mechanics energy, the solvation free energy, and the conformational entropy upon binding at a certain temperature T , respectively. ΔE_{MM} includes $\Delta E_{\text{internal}}$ (bond, angle, and dihedral energies), electrostatic, and van der Waals energies, and the term is the difference in energy between the complex structure and the sum of the ligand energies and the receptor alone. ΔG_{sol} is the electrostatic solvation energy $\Delta G_{\text{PB/GB}}$ (polar contribution) and nonelectrostatic solvation component ΔG_{SA} (nonpolar contribution) sum; this term corresponds to the difference in the GBSA solvation energy of the complex and the solvation energies for the ligand and the unliganded receptor sum. The polar contribution is calculated using the generalized Born model, while the nonpolar energy is calculated by solvent accessible surface area (SASA).^{52,53} Corrections for entropic changes were not applied because here we used MM-GBSA to rescore docking poses and not to estimate the real binding free energy of A1899 and TASK-1 channel. It has repeatedly been

suggested that the entropy term does not improve the results of MM-GBSA binding free energy calculation in large tests.^{54–58}

Experimental Interaction Scoring. According to the alanine mutagenesis screening (AMS) results previously reported,²⁷ we assigned a score for each interaction between A1899 and the residues of the binding site for each A1899 conformation. The experimental interaction score (EIS) represents the sum of the contribution to the inhibition obtained by AMS for each amino acid when the block by 400 nM A1899 was analyzed. EIS was normalized in such a way that residues contribution to the binding site sum 100 (Thr⁹², 5.7; Thr⁹³, 9.8; Ile¹¹⁸, 12.4; Leu¹²², 7.3; Thr¹⁹⁸, 7.4; Thr¹⁹⁹, 8.5; Ile²³⁵, 7.5; Gly²³⁶, 6.8; Leu²³⁹, 11.8; Asn²⁴⁰, 8.1; Val²⁴³, 7.5; and Met²⁴⁷, 7.1). Accordingly, we analyzed the interactions of all A1899 poses from docking; for instance, the pose 1 (Table S2) interacts with Thr⁹² (5.7); Thr⁹³ (9.8); Ile¹¹⁸ (12.4); Leu¹²² (7.3); Leu²³⁹ (11.8); Thr¹⁹⁸ (7.4); Thr¹⁹⁹ (8.5); Gly²³⁶ (6.8); Asn²⁴⁰ (8.1); and Val²⁴³ (7.5); therefore the EIS is 85.3.

Clustering of Conformers. A total of 800 poses (10 poses for each frame, 20 frame for each model, 4 different TASK-1 models) was obtained. To process and to organize the 800 poses we used the Conformer Cluster script (available in www.schrodinger.com/scipcenter/). This script builds a matrix⁵⁷ using a measure of pairwise distance between conformations. This measure was the root-mean-square displacement (RMSD) between pairs of corresponding atoms following optimal rigid-body superposition.⁵⁹ The atomic RMSD was calculated considering the atoms from A1899 numbered in Figure S2B, and the linkage average method was used to cluster the A1899 poses.

Molecular Dynamics Simulations. The eight complexes A1899–TASK-1 with the best ΔG_{bind} and EIS were subjected to a conjugate gradient energy minimization and MDs in Desmond v3.0 using OPLS-2005^{34,35} force field. The receptor–ligand complexes were embedded into a POPC lipid bilayer and were solvated by an orthorhombic box of SPC water model, covering the whole surface of each system. Cl[−] ions were used as counterions in order to neutralize the systems, and a 0.096 M concentration of KCl was added to match the concentration used in electrophysiological measurements of A1899 on TASK-1.²⁷ The temperature was maintained at 300 K, while pressure was kept at 1 atm, employing the Nose–Hoover thermostat method with a relaxation time of 1 ps using the MTK algorithm.⁶⁰ Data were collected every 5 ps during the MDs for further analysis. We performed two MDs for each A1899–TASK-1 complex. For the first 40 ns, simulation was performed with application of a restraint spring constant of 0.5 kcal mol^{−1} Å^{−2} to the secondary structure of the receptor; then, the last frame was taken and a second nonrestricted 100 ns MDs was performed. For the TASK-1 homology model T1trOO, two MDs—one with the ligand and one without it—using the same protocol described above were performed.

Oocyte Preparation, cRNA Synthesis, and Injection. Oocytes were obtained from anesthetized *Xenopus laevis* frogs and incubated in OR2 solution containing (in mM) NaCl 82.5, KCl 2, MgCl₂ 1, and HEPES 5 (pH 7.5), supplemented with 2 mg/mL collagenase II (Sigma) to remove residual connective tissue. Subsequently, oocytes were stored at 18 °C in ND96 solution containing (in mM) NaCl 96, KCl 2, CaCl₂ 1.8, MgCl₂ 1, and HEPES 5 (pH 7.5), supplemented with 33.6 μM gentamycin, 2.5 mM sodium pyruvate, and 0.5 mM theophylline. Human TASK-1 (KCNC3, NM_002246) was subcloned into the oocyte expression vector pSGEM. Mutations were

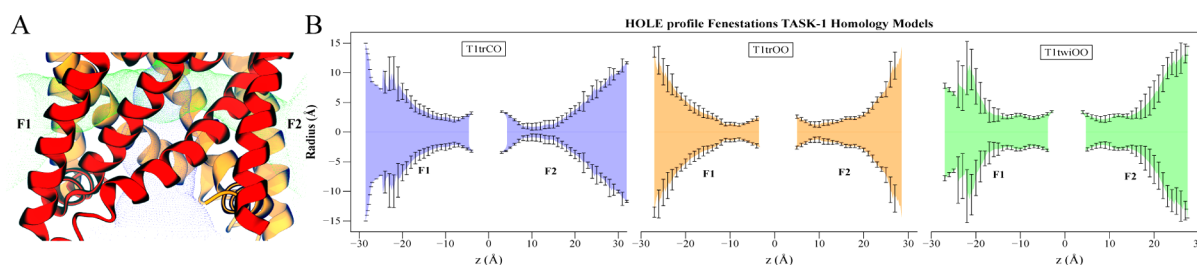


Figure 1. Characterization of the side fenestrations in TASK-1 models. HOLE profiles of the fenestrations for the TASK-1 models derived from 10 ns MDs. (A) Representation of the fenestrations F1 and F2 (green dotted surface) connected to a portion of the inner pore at the bottom of the selectivity filter (blue dotted surface) in the T1twOO model. Subunits A (orange) and B (red) are shown in cartoon representation. (B) Graphs show the average diameter and the standard deviation of the fenestrations in T1trCO (blue), T1trOO (orange), and T1twOO (green) models for each MDs (20 structures from each MD—0.5 ns frames each—were taken). F1 left, F2 right. The bottleneck diameters are at the following positions in the z-axis in each model. T1trCO: F1 z-axis = -8 \AA and F2 z-axis = 10 \AA . T1trOO: F1 z-axis = -8 \AA and F2 z-axis = 10 \AA . T1twOO: F1 z-axis = -7 \AA and F2 z-axis = 8 \AA .

introduced with the QuickChange Site Directed Mutagenesis Kit (Stratagene) according to the manufacturer's instructions. Subsequently, cDNA was linearized and cRNA was synthesized with the mMESSAGING mMACHINE-Kit (Ambion). The quality of cRNA was tested using agarose gel electrophoresis. cRNA was quantified using a UV-vis spectrophotometer (NanoDrop 2000). Oocytes were each injected with 50 nL (5 ng) of cRNA.

Electrophysiology. Two electrode voltage clamp (TEVC) recordings were performed 48 h after cRNA injection at room temperature ($20\text{--}22 \text{ }^\circ\text{C}$) with a TurboTEC 10CD (npi) amplifier and a Digidata 1200 series (Axon Instruments) as A/D converter. Micropipettes were made from borosilicate glass capillaries GB 150TF-8P (Science Products) and pulled with a DMZ-Universal Puller (Zeitz). Recording pipettes had a resistance of $0.5\text{--}1.5 \text{ M}\Omega$ and were filled with 3 M KCl solution. ND96 was used as recording solution. Inhibition by 400 nM A1899 was analyzed with voltage steps from a holding potential of -80 mV . A first test pulse to 0 mV of 1 s duration was followed by a repolarizing step to -80 mV for 1 s, directly followed by another 1 s test pulse to $+40 \text{ mV}$. The sweep time interval was 10 s. Wash in was studied at $+40 \text{ mV}$. For current-voltage (IV) curves, voltage was ramped from -120 to $+45 \text{ mV}$ within 3.5 s from a holding potential of -80 mV . Bath exchange time was determined from experiments in which the pipet offset was continuously recorded when switching from a water containing solution to a high potassium solution.

RESULTS

Characterization of the Side Fenestrations in TASK-1 Models. To simulate the behavior of TASK-1 within a lipid membrane, and considering the different conformation and fenestration states of the crystallized K_{2P} channels, we built four homology models: T1treCC, T1twOO, T1trOO, and T1trCO (Experimental Section and Table 1). All models were subjected to 10 ns MDs. The RMSDs of the position for all backbone atoms of the TASK-1 models from their initial configuration as a function of simulation time are illustrated in Figure S4. All models were equilibrated after 1 ns of MDs. The RMSD values remain within 0.65 \AA for all TASK-1 models, demonstrating the conformational stabilities of the receptor structures.

For each MDs, 20 structures (0.5 ns frames each) were taken. In total we collected 80 structures from the TASK-1 homology models MDs. All structures were analyzed with the HOLE algorithm to gain insight into the putative relevance of the fenestrations for the interaction of A1899 with the TASK-1 channel. The fenestrations (F1, F2) formed at the interface

between the subunits A (orange) and B (red) are illustrated in Figure 1A. HOLE radius profile analysis (along the 10 ns MDs) showed differences in diameter between the three models exhibiting open fenestrations: T1trCO, T1trOO, and T1twOO (Figure 1B). T1trCO presents F1 (left) open with a bottleneck diameter (BD) of $4.25 \pm 0.91 \text{ \AA}$ in contrast to F2 (right), which is closed and has a BD of $1.79 \pm 1.07 \text{ \AA}$. In T1trOO the fenestrations showed a BD of $2.44 \pm 0.71 \text{ \AA}$ in F1 and $2.57 \pm 0.98 \text{ \AA}$ in F2. In the case of T1twOO, its fenestrations exhibited the largest BD compared to the other two models mentioned above, $4.82 \pm 0.71 \text{ \AA}$ in F1 and $4.36 \pm 0.99 \text{ \AA}$ in F2.

Next we analyzed the position of residues previously identified as forming part of the A1899 binding site.²⁷ In more detail, we studied Thr⁹² and Thr⁹³ in the P1 region, Thr¹⁹⁸ and Thr¹⁹⁹ in the P2 region, Ile¹¹⁸ and Leu¹²² in the M2 segment, Leu²³², Ile²³⁵, Gly²³⁶, Leu²³⁹, and Asn²⁴⁰ in the M4 segment; and Val²⁴³ and Met²⁴⁷ in the halothane response element (HRE). We examined for each model the relative presence of these amino acids during the MDs in the central cavity and/or fenestrations using the HOLE algorithm.³⁷ Table 2 summarizes whether the residues of the A1899 binding site face into the fenestration and/or the pore.

Unexpectedly from the initial description of the A1899 binding site using a KvAP open state model of TASK-1, only the residues Thr⁹³, Asn²⁴⁰, and Met²⁴⁷ are exclusively present in

Table 2. HOLE Results. Residues in the Fenestration (F) and the Pore during the MDs^a

residue	T1treCC	T1trCO	T1trOO	T1twOO
Thr ⁹²	NP	NP	NP	NP
Thr ⁹³	pore	pore	pore	pore
Ile ¹¹⁸	NP	F	F	F
Leu ¹²²	pore	pore, F	pore, F	pore, F
Thr ¹⁹⁸	NP	F	F	F
Thr ¹⁹⁹	pore	pore, F	pore, F	pore, F
Leu ²³²	NP	NP	F	F
Ile ²³⁵	NP	F	F	F
Gly ²³⁶	NP	F	F	F
Leu ²³⁹	NP	F	F	pore, F
Asn ²⁴⁰	pore	NP	pore	pore
Val ²⁴³	NP	NP	NP	NP
Met ²⁴⁷	pore	pore	NP	NP

^aA residue is considered as part of a cavity if it remains more than 50% of the MDs time in the cavity. NP: No presence.

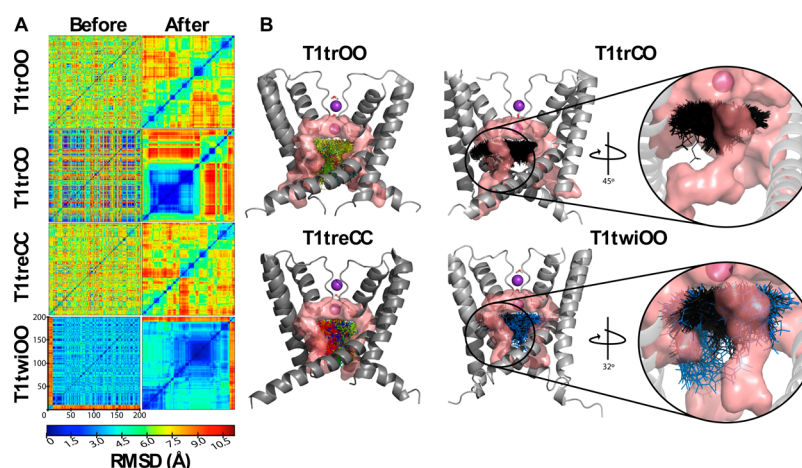


Figure 2. Ordering of A1899 docking solutions in TASK-1 by cluster analyses. Clustering of A1899 poses was performed by atomic RMSD comparison. (A) The symmetrical distance matrix illustrates atomic RMSD comparison of the 200 poses of A1899 found by molecular docking per model. On the diagonal line the RMSD is zero because the poses are compared with themselves. Left: Matrix of A1899 poses organized by number before clustering. Right: Matrix of A1899 poses after clustering. The poses are organized using atomic RMSD. The input order is kept on the diagonal; accordingly, the significant clusters are now visible as squares on the line. The inferior bar is the RMSD atomic distance scale in Å. Table S3 shows all the clusters of A1899 poses per model, the mean cluster population, and the associated standard deviation (σ). (B) Significant clusters are represented by colored lines. K^+ ions are shown in sphere representation and TASK-1 models in cartoon representation. For clarity only the segments P1, M1, and M2 are shown. The binding site is represented in pink surface representation. Clusters no. 17 (black) and no. 18 (blue) interacting with T1twiOO and cluster no. 57 (black) interacting with T1trCO are zoomed for a better visualization.

the central cavity of the channel during the MDs. Residues Leu¹²², Thr¹⁹⁹, and Leu²³⁹ are present both in the pore and in the fenestrations. In addition, unlike in our previous study, which lacked a K_{2p} crystal structure as a modeling template,²⁷ we observed that the residues Ile¹¹⁸, Thr¹⁹⁸, Leu²³², Ile²³⁵, and Gly²³⁶ were exclusively oriented toward the fenestrations and did not protrude into the central cavity.

In a model with closed fenestrations (T1treCC) 5 out of 13 of the residues belonging to the experimentally determined binding site are present in the central cavity, with the other residues hidden inside the protein. Also in models with open fenestrations, the majority of the binding site residues are not facing the central cavity, but point into the lateral openings: 7 out of 13 of the residues in T1trCO, and 8 out of 13 in both T1trOO and T1twiOO models. Only 4 out of 13 of the binding site residues are present in the pore in both T1trCO and T1trOO models, and 5 in T1twiOO (Table 2).

Ordering of A1899 Docking Solutions in TASK-1 by Cluster Analyses. To study the interaction of A1899 with TASK-1 in the four different TASK-1 homology models, we considered the flexibility of the residues of the structures, especially those of the binding site. For this purpose, we performed docking assays in the 80 frames obtained from the four TASK-1 homology models during the 10 ns MDs. The structures were prepared for molecular docking simulations retaining the structural and energetic properties from the MDs. The top 10 poses for each docking were saved. With this protocol we collected 200 poses of A1899 for each of the four TASK-1 models (800 in total). All poses were clustered using a RMSD matrix (see Experimental Section). Figure 2A shows the RMSD matrices before and after grouping into clusters by conformational similarities. Significant conformational clusters, for which the populations depart by more than 2σ from the mean cluster population,⁶¹ are summarized in Table 3. Figure 2A illustrates the significant clusters and their size as blue squares, visible on the diagonal lines. The significant clusters within the different TASK-1 models, located in the central

Table 3. Significant Clusters of All Models with the Population and Average Docking Energy

model	no. of cluster	population	av docking energy (kcal mol ⁻¹)
T1treCC	1	37	-48,392
	2	31	-51,927
	3	23	-47,410
	4	23	-50,966
T1twiOO	17	67	-48,712
	18	45	-49,873
T1trOO	36	26	-49,706
	37	26	-47,979
	38	20	-49,878
	39	18	-48,945
T1trCO	40	17	-49,347
	57	93	-51,124

cavity and/or fenestrations, are depicted in different colors (Figure 2B). From the clustering process it can be seen that A1899 poses docked in T1twiOO exhibit a lower RMSD than in other models (Figure 2A). The most populated clusters of A1899 in the T1twiOO model (Table 3), Cluster-17 (black) and Cluster-18 (blue), are located within the fenestrations (Figure 2B zoom). Also cluster no. 57 (Table 3) of the T1trCO model, which has 93 conformations (the highest population of all the clusters we identified), is oriented inside the open fenestration F1 (Figure 2B zoom). These open hydrophobic fenestrations allow the ligand (LogP value = 4.738) to anchor inside. Accordingly, the T1trCO and T1twiOO structures which have side fenestrations with a larger diameter (Figure 1B) have increased populations within their clusters.

Ordering A1899 Poses of Significant Clusters by Their MM-GBSA Binding Free Energy. A1899 poses from the significant clusters were further analyzed and rescored by their MM-GBSA free binding energy, ΔG_{bind} (kcal mol⁻¹). In Figure 3A we plot the experimental interaction score (EIS) against the ΔG_{bind} for all A1899 poses within significant clusters. The framed poses in the top left corner represent the best docking

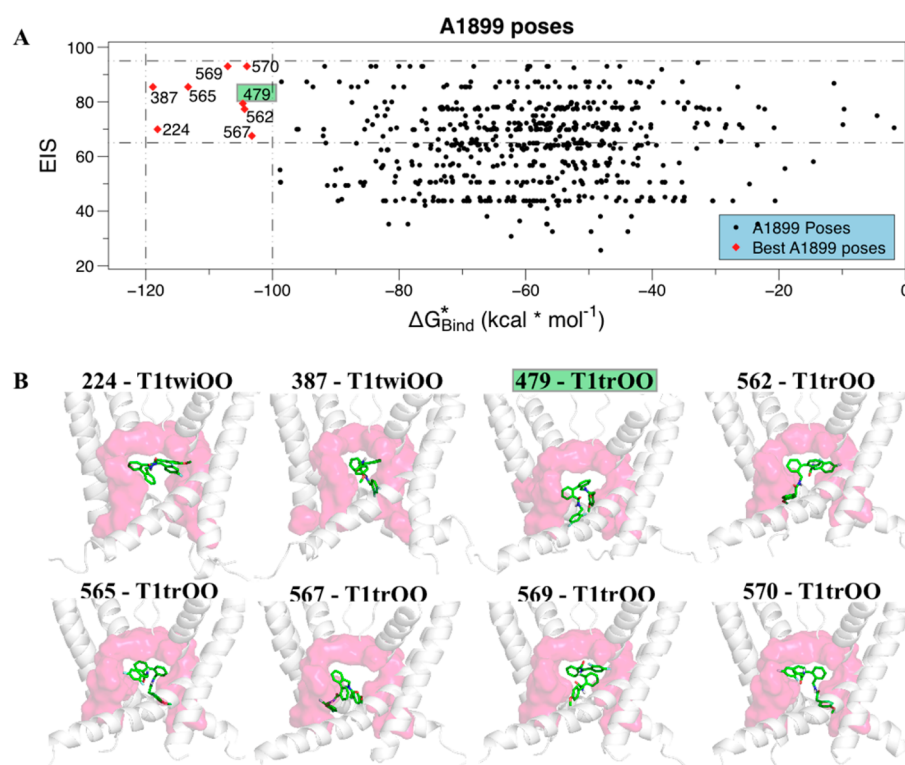


Figure 3. Ordering A1899 poses of significant clusters by their MM-GBSA free binding energy. (A) ΔG_{bind} energy vs experimental interaction score plot of the A1899 poses of significant clusters are represented in black dots. The best A1899 poses are represented in red dots. In Table S2 the ΔG_{bind} for each pose in the significant clusters is given. The best pose selected for further experiments, as it reflects all the functional data from a previous mutagenesis study,²⁷ is highlighted with a green square (pose 479). (B) A1899 best poses in stick representation interacting with TASK-1 models (cartoon representation); only the segments P1, M1, and M2 are shown. The binding site described previously by mutagenesis study²⁷ surrounding each A1899 conformation is illustrated in pink surface representation.

solutions according to their lower ΔG_{bind} value (between -120 and -100 kcal mol⁻¹) and their higher EIS (between 65 and 95). The best A1899 poses are found for models in which both fenestrations are in the open state. For instance, 224 and 387 are from T1twiOO, and poses 479, 562, 565, 567, 569, and 570 are from the T1trOO model (Figure 3A,B).

The analysis of all A1899 poses from the significant clusters (black dots in Figure 3A) reveals that the drug is mostly oriented perpendicular to the pore, consistent with a direct blockage of the ion flux through the channel. This becomes also evident from the best docking solutions illustrated in Figure 3B. We found that residues Thr⁹³ and Thr¹⁹⁹ located at the base of the selectivity filter are relevant for these interactions. 95.1% and 98.8% of the poses interact with residues Thr⁹³ and Thr¹⁹⁹, respectively. This interaction with A1899 probably occurs through H-bonds. Analyzing all complexes with the four different models, a total of 56 H-bonds are found to be present in the interaction between A1899 and Thr⁹³ and a total of 26 H-bonds in the interaction with Thr¹⁹⁹. Note that the T1treCC model, the only one with a closed–closed fenestration state, presents only one pose (pose 161) with a H-bond to Thr⁹³ (Table S2). This phenomenon probably indicates that fenestrations may strengthen the interactions between A1899 and TASK-1.

To study how A1899 interacts with the residues of the binding site, the complexes of A1899 with TASK-1 having the lowest ΔG_{bind} energy and the highest EIS (poses 224, 387, 479, 562, 565, 567, 569, and 570; Figure 3A) were selected and subjected to MDs. The atomistic systems were equilibrated and relaxed for 40 ns. Then, the relaxed complexes were subjected

to 100 ns unrestrained MDs. In all MDs the TASK-1 structure remained stable (Figure S5A), even for the A1899–TASK-1 complex (pose 387). The A1899 poses were stable during the MDs, and the structures showed only minor deviations from their initial docking positions (Figure S5B).

Contacts of A1899 with Residues of the TASK-1 Binding Site and the Nature of the Chemical Interactions. We analyzed how frequently A1899 interacts with the residues of the binding site during the 100 ns MDs. To this end the contact frequencies of A1899 were calculated by looking at the residues within less than 4 Å distance to the ligand. Of all the samplings along the fitted simulation time, A1899 pose 479 was the conformation that correlated better with the experimental data reported previously, as transient interactions along the MDs were established with all the residues of the binding site described by Streit et al.,²⁷ including with Met²⁴⁷, which had not been predicted by docking (Figure 4A).

To characterize changes in the A1899 heavy atoms position along the 100 ns unrestrained MDs of our final model (pose 479 from the T1trOO model), the RMSF (root-mean-square fluctuation) was calculated. RMSF shows the stability of the ligand along the MDs due to the established interactions with the residues of the binding site. The low RMSF values indicate that A1899 remains in the binding site during the whole MDs (Figure S6A,B). This is in agreement with the stable time dependence of RMSD for A1899 in our model (Figure S5A) and indicates that A1899 has not undergone a major rearrangement of its conformation during the MDs (Figure S5B).

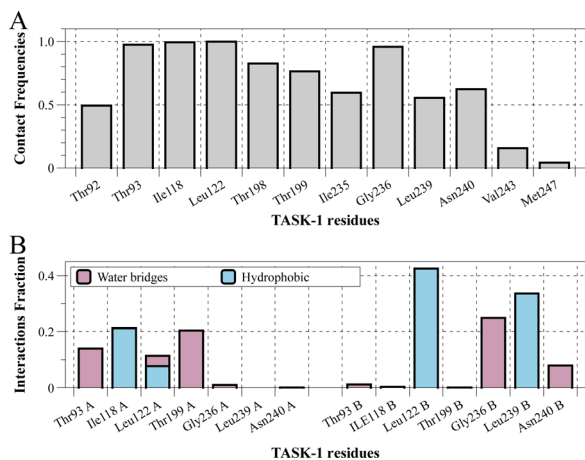


Figure 4. Contacts of A1899 with residues of the TASK-1 binding site during the 100 ns MDs and the nature of the chemical interactions. (A) A1899 pose 479 is at 4 Å of all the binding site residues. Contact frequencies of A1899 with T1trOO residues at 4 Å. Bars indicate the contact frequency along the 100 ns MDs. (B) Interactions between the residues of T1trOO and A1899 pose 479 are categorized into two types: hydrophobic and water bridges. The stacked bar charts are normalized over the course of the unrestrained MDs.

We also analyzed the chemical nature of the A1899 interaction with TASK-1 over the time period of the unrestricted MDs. The data were categorized and summarized into two types: hydrophobic and water bridges (Figure 4B). The stacked bar charts were normalized over the course of the trajectory. It can be seen that although pose 479 is within 4 Å from all the residues of the binding site, not all of them interact chemically with A1899. Only Thr⁹³, Leu¹²², and Thr¹⁹⁹ from subunit A and Gly²³⁶ and Asn²⁴⁰ from subunit B form water

bridges with the drug through H-bonds. Residues Ile¹¹⁸ and Leu¹²² from subunit A and Leu¹²² and Leu²³⁹ from subunit B interact with A1899 via hydrophobic contacts (Figure 4B). This network of hydrophobic and water bridges interactions allows A1899 to block the K⁺ flux due to its conformational location at the bottom of the SF (Figure 5).

A1899 Stabilizes the Open Fenestrations of TASK-1.

To study how the fenestrations change over time due to the presence of A1899, HOLE radius profiles were determined for the T1trOO model and the A1899–T1trOO complex after 0 and 100 ns of the unrestricted MDs. A1899 is located in the inner cavity protruding into fenestration F2. At the beginning of MDs (0 ns, green) both fenestrations were open. With A1899 the F1 fenestration remains unchanged but F2 changed and opened by an additional 4 Å (after 100 ns, blue), indicating that the ligand favors the fenestration open state despite its location in the inner cavity. This phenomenon can be appreciated at 16.2 Å in the z-axis (Figure 6).

A1899 Does Not Pass the Side Fenestrations To Reach the Binding Site.

To determine if A1899 can go from the membrane through the fenestrations to its binding site, we experimentally blocked the fenestrations by individually mutating the residues Leu¹¹⁵ and Phe²³⁸ to tryptophan, as these large moieties will project into the fenestration lumina markedly decreasing their diameter. That both L115W and F238W mutations are likely to close the fenestrations (Figure 7A) can be seen by analyzing the HOLE radius profiles of the mutant models in comparison with the wild-type channel model. At position 16.25 Å of the z-axis where the fenestration diameter in WT is 6.34 Å, that of L115W is decreased to 4.18 Å and that for F238W mutant to 2.76 Å (Figure 7B). In voltage clamp recordings, the mutants are inhibited as efficiently as wild-type TASK-1 by 400 nM A1899 (Figure 7C,D), as

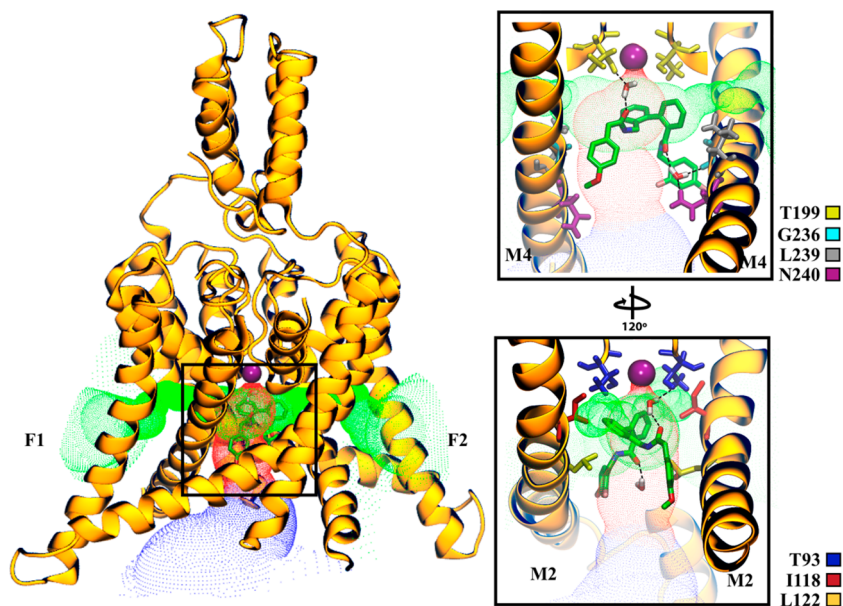


Figure 5. Redefined binding mode of A1899 in TASK-1 includes residues that contribute to the side fenestrations. Residues Thr⁹³ (blue) from P1 and Asn²⁴⁰ (magenta) from M4 segment are exclusively in the pore. Residues Leu¹²² (yellow) from M2 and Thr¹⁹⁹ (light yellow) from P2 are facing the pore and the fenestrations; Gly²³⁶ (cyan) and Leu²³⁹ (gray) from the M4 segment and Ile¹¹⁸ (red) from M2 are exclusively in the fenestrations (Table 2). All the amino acids as well as the water molecules are shown in stick representation. The H-bond interaction between A1899–Thr⁹³, A1899–Thr¹⁹⁹, A1899–Gly²³⁶, and A1899–Asn²⁴⁰ through water bridges are shown as black dotted lines. Fenestrations are shown as green dotted surface, and the inner pore region where A1899 is interacting is shown as a red dotted surface; the rest of the inner pore is shown as a blue dotted surface.

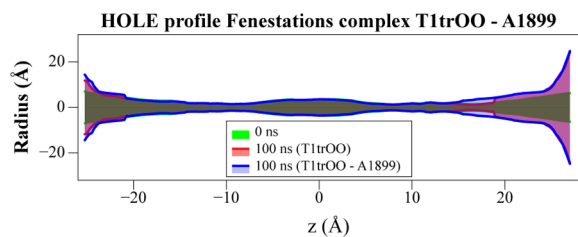


Figure 6. A1899 stabilizes the open fenestrations of TASK-1. A1899 pose 479 protrudes into the side fenestration F2. HOLE radius profile of the T1trOO fenestrations at the start of the MDs (0 ns, green) and after 100 ns with (blue) and without (red) A1899. The bottleneck diameters at F2 are as follows: T1trOO, 0 ns, BD = 2.29 Å, z-axis → 16.7 Å; T1trOO, 100 ns, BD = 2.29 Å, z-axis → 16.7 Å; T1trOO + A1899, 100 ns, BD = 6.34 Å, z-axis → 16.2 Å.

expected, given that these residues do not directly contribute to A1899 binding. Importantly, however, occlusion of the intramembrane fenestrations by the tryptophane side chains did not alter the kinetics for the onset of inhibition. This suggests that the intramembrane fenestrations are not an important pathway for drug access to its binding site in the central cavity (Figure 7E). The onset of block in our experimental setting includes time for drug application, drug mixing in the bath, and slow diffusion through the vitelline membrane. Given the very slow off rate of A1899 in this voltage clamp setting²⁷ compared to the relatively fast bath exchange, an additional prominent delay in the onset of inhibition by limited or restricted diffusion through the side fenestrations should have become evident. Effective bath exchange is

completed in less than 1 min, while drug block requires several minutes.

DISCUSSION

A key feature of K_{2P} channels is the presence of intramembrane side fenestrations located just underneath the selectivity filter that, according to the recent literature, could be “druggable”.⁶² In our study we probed whether the TASK-1 specific blocker A1899 is utilizing these fenestrations to cause channel inhibition. To study the interaction of A1899 with TASK-1 in four different TASK-1 homology models with different fenestration states, we considered the flexibility of the binding site residues, and collected 200 poses of A1899 for each one of the models (800 in total). We then faced the problem of choosing a single binding mode from several different docking conformations. The model had to reflect, in addition, details about the binding of A1899 to the channel as uncovered by our previous experimental results.²⁷ Often, docking scoring functions might not help with the choice.^{45,46} To tackle this issue, it was proposed to utilize a clustering approach.⁶¹ The pose 479 selected belongs to cluster #40 with a population of 17 conformations docked into the T1trOO model (Table 3 and Table S3). As expected from our previous work A1899 pose 479 blocks the K^+ flux due to its conformational location underneath the selectivity filter (Figure 5). However, the ligand, despite being located in the central cavity, favors a binding to open fenestrations (Figure 6).

Almost all the poses of A1899 are located underneath the selectivity filter. These results are in concordance with those reported by Kiper et al.²⁶ in their study of the interaction of A1899 and other biphenyl derivatives such as AVE01118 and

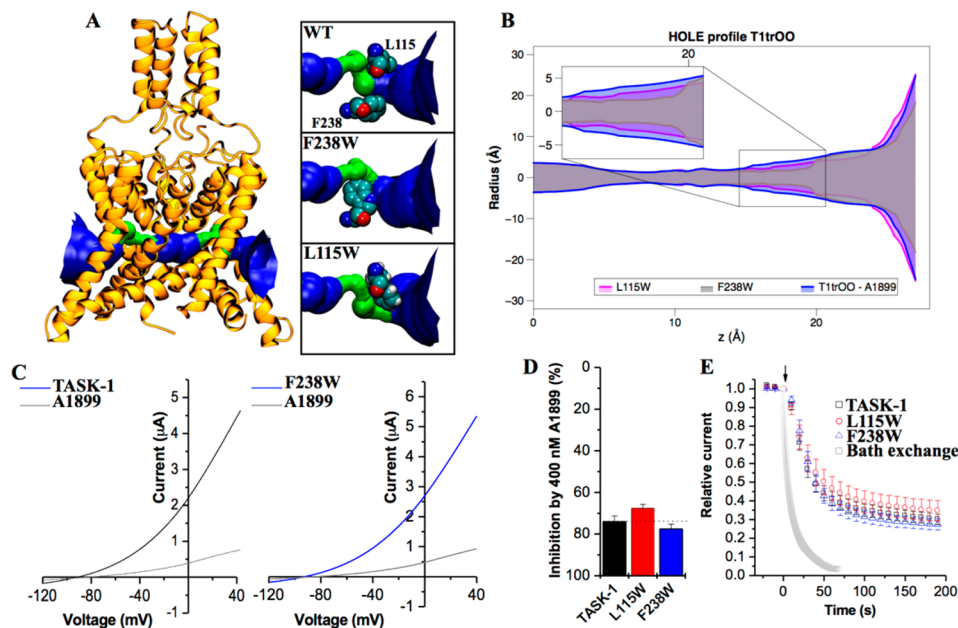


Figure 7. A1899 does not pass the side fenestrations to reach the binding site. Replacement of Leu¹¹⁵ and Phe²³⁸ by tryptophan reduces fenestration radii. (A) Surface representation of the fenestrations of T1trOO-WT (corresponds to T1trOO–A1899 after 100 ns of MDs), L115W, and F238W residues are shown in sphere representation. The *in silico* mutations were done at the structure of T1trOO–A1899 after 100 ns of MDs. Fenestration radii > 2.30 Å (blue), fenestration radii < 2.30 Å (green). (B) HOLE radius profile of T1trOO–A1899–L115W (pink), T1trOO–A1899–F238W (gray), and T1trOO–A1899 (blue); only fenestration F2 is represented. (C) TEVC recordings of TASK-1 (black) and TASK-1 F238W (blue) before and after application of 400 nM A1899 (gray). (D) Percentage of block by 400 nM A1899 of TASK-1 wild-type (black) or the mutants L115W (red) and F238W (blue) analyzed at +40 mV. (E) Wash-in kinetics of A1899 of TASK-1 wild-type (black) and the mutants L115W (red) and F238W (blue). Gray squares indicate the average effective speed of bath exchange determined by measuring microelectrode offset change elicited by switching to a KCl solution into a water-filled bath chamber ($n = 6$).

S9947 with TASK-1. Kiper et al.²⁶ proposed a common pharmacophore for A1899, AVE01118, and S9947 including two H-bond acceptors and one aromatic ring. The authors suggested that these common chemical features correspond to a shared binding mode in TASK-1, located at the bottom of the selectivity filter, rather remote from the distal part of the M4 segment, including the residue Met²⁴⁷ of the TASK-1 binding site for A1899.²⁷ Streit et al., 2011,²⁷ could not explain the interaction of A1899 with the remote Met²⁴⁷ and therefore suggested that this residue might be only relevant as it is located in the pathway to the central cavity. But here, as we explored eight-hundred A1899 conformations, we found a pose (479) within 4 Å from all the residues of the binding site including Met²⁴⁷ (Figure 4A). Therefore, our final binding model of A1899 could also be a starting point to study the structural differences in the drug affinities of TASK-1 and TASK-3 channels, given that Met²⁴⁷ is the only amino acid of the A1899 binding site not conserved in TASK-3 that has a Leu residue at the homologous position. Chokshi et al.²⁸ studied the PK-THPP, A1899, and doxapram binding sites in TASK-3 channels, and found that mutation L247D impacts PK-THPP potency. Note that the authors also observed that L122D, G236D, L239D, and V242D mutations impair A1899 and doxapram inhibition in TASK-3. In contrast, we did not identify Val²⁴² as a relevant residue for the binding of A1899 in TASK-1. In all our TASK-1 models generated in the current study Val²⁴² does not face toward the pore. From the unrestrained MDs performed for the best docking solutions according to their lower ΔG_{bind} value (Figure 3A), only pose 387 exhibits a 10.7% of contact frequency interaction with Val²⁴² at 4 Å (data not shown). The docking experiments reported by Chokshi et al. illustrate how A1899 binds to TASK-3 deeper in and across the pore with its difluorophenyl moiety interacting with several aliphatic residues at the fenestration. The best docking pose of A1899 reported in the present study (479) is not interacting with TASK-1 in the same way (Figure 5), a fact that might in part explain the different affinities for TASK-1 and TASK-3. Pose 479 during the unrestricted MDs is interacting with TASK-1 through a network of water bridges and hydrophobic interactions along both pore and fenestration cavities. The water bridges are established between both oxygens from the carbonyl groups of A1899 through two water molecules with the threonines located at the bottom of the SF (Thr⁹³ and Thr¹⁹⁹) as well as with the Asn²⁴⁰ in the pore and Gly²³⁶ at fenestration F2. The difluorophenyl and the *p*-phenyl methoxy moieties present nonpolar interactions with pore residue Leu¹²² and with Ile¹¹⁸, Leu¹²², and Leu²³⁹ at the fenestration (Figure 4B). It is worth highlighting that Leu¹²² is located in both pore and fenestration cavities (Table 2) allowing a dynamic interaction of A1899, like the biphenyl moiety which interacts within the pore and with fenestration F2 (Figure 5).

It has been previously suggested that Met²⁴⁷ might influence drug sensitivity because it regulates the accessibility of A1899 to the pore. As A1899 was able to tightly bind to TASK-1 models with open fenestrations, and these lateral cavities can potentially work as drug access pathways,⁶² we wondered whether Met²⁴⁷ regulates A1899 access to the pore or whether the compound travels a completely different way entering the central cavity via the side fenestrations. When residues Leu¹¹⁵ and Phe²³⁸, which are exposed to the lateral cavities in the homology models, are replaced by voluminous residues, the respective mutants are inhibited by A1899 just as efficiently and with the same kinetics as wild-type TASK-1 (Figure 7). These

data suggest that A1899 does not travel laterally from the lipid face through the side fenestrations to reach the binding site.

The lateral fenestrations in K_{2P} channels are only present in what has been called the “down state”, which refers to the position of the M4 segment that extends intracellularly in a rather straight way. In the “up state”, the fenestrations are closed by the upward movement and rotation of M4.¹¹ All of our TASK-1 homology models exhibit different fenestration shapes; in fact, these structural differences appear to play a major role in the interaction between A1899 and TASK-1. In the model with closed fenestration states (T1treCC) the sole possibility is for an interaction of A1899 at the base of the selectivity filter. The open fenestrations in T1trCO and T1twiOO, on the other hand, allow A1899 hydrophobic moieties to be oriented toward the interior of the fenestrations (Figure 2B, zoom view). The T1trOO fenestrations are not large enough to allow the complete entry of A1899 into the fenestrations (Figure 1B). We observed A1899 average poses of the five significant clusters in T1trOO (Table 3), and all of them are placed in the central cavity (Figure S7) but anchored by the residues of the binding site located at the fenestrations in T1trOO (Table 2). A mechanism in which blockers acting at the central cavity require lateral interactions anchoring them to residues in the side fenestrations might be conserved among K_{2P} channels, as the relevant residues forming the fenestrations share high sequence similarities within the K_{2P} channel family.^{9,62}

The relevance of the structural differences in the fenestrations for the interaction of A1899 with TASK-1 is also supported by the number of binding site residues that become available in the open fenestrations. In a model with a closed fenestration state (T1treCC) A1899 would be able to interact with only 5 out of 13 binding site residues, i.e., those present in the central cavity. In contrast, in models with lateral fenestrations interactions with binding site residues located within these structures become possible: these represent 7 out of 13 of the TASK-1 binding site residues in T1trCO, and 8 residues in both T1trOO and T1twiOO models (Table 2).

Streit et al. previously reported that A1899 acts as an open-channel blocker and binds to residues of the P1 and P2 regions, M2 and M4 segments, and the halothane response element (HRE) in TASK-1 channel.²⁷ The mode of A1899 binding was modeled using an open state KvAP crystal structure as a template as no K_{2P} structures were available at the time. That TASK-1 homology model had a 4-fold symmetry and lacked side fenestrations. Although A1899 can bind to structures with closed fenestrations such as T1treCC, our data suggests a redefinition of the A1899 binding mode, in which the blocker additionally binds tightly to structures within the open fenestrations. TASK-1 open probability increases with depolarization,⁶³ suggesting that there are more channels in the up state with closed fenestrations. However, A1899 is not a state-dependent blocker, because there was no voltage dependence of inhibition.²⁷ In fact no reduced block was observed during depolarization, which one would expect for a preferential binding to the down state with open fenestrations. On the other hand our data suggest that, once A1899 has bound and blocked TASK-1, the closed state of the channel with open fenestrations is more favorable. This becomes evident (1) as in open fenestration structural models all the residues of the binding site can participate in drug binding and (2) as we found in MDs, an opening of the fenestrations occurs in the presence of A1899 (Figure 6). This stabilization of the closed state might

be directly mediated by residues of the drug binding site in or near the fenestrations, i.e., Ile²³⁵ and Leu²³⁹, as the homologous residues in TWIK-1 (Met²⁶⁰ and Leu²⁶⁴) were reported to be crucial for the equilibrium between open and closed fenestration states.⁶² Taken together these data suggest that A1899 can bind to both the open and the closed fenestration states and that the drug will stabilize the closed state after pore block.

In the present work, we have developed a systematic pipeline (Scheme 1) that includes different homology models with different conformations along a fitted simulation time. Massive dockings, clustering of conformers, and MM-GBSA binding free energy calculations, followed by long MDs, have allowed us to explore and to describe properly the TASK-1 accessible conformational landscape for the interaction with A1899. This scheme is more effective in sampling the full range of conformational space of ligands compared to the individual application of each of the methods used here alone.

In summary, we demonstrate that the TASK-1 specific blocker A1899 requires a binding to residues that are located in the side fenestrations. Unexpectedly, the majority of residues previously described to interfere with TASK-1 block by A1899 project their side chains toward the fenestration lumina, underlining the relevance of these structures for drug binding in K_{2P} channels. Despite its hydrophobicity, A1899 does not seem to use the fenestrations to gain access to the central cavity from the lipid bilayer. In contrast, binding of A1899 to residues of the side fenestrations might provide a physical “anchor”, reflecting an energetically favorable binding mode that stabilizes the closed state of the channels after pore occlusion.

■ ASSOCIATED CONTENT

📄 Supporting Information

The Supporting Information is available free of charge on the ACS Publications website at DOI: 10.1021/acs.molpharmaceut.7b00005.

PDB files of the TASK-1 homology models (ZIP)

Figures S1–S7, Tables S1–S3, and references (PDF)

■ AUTHOR INFORMATION

Corresponding Authors

*W.G.: Centro de Bioinformática y Simulación Molecular, Universidad de Talca, 1 poniente No. 1141, 3460000, Talca, Chile. Tel: (+56) 712201674. E-mail: wgonzalez@utalca.cl.

*N.D.: Institute for Physiology and Pathophysiology, Vegetative Physiology, Philipps-University of Marburg, Deutschhaustraße 1-2, 35037 Marburg, Germany. Phone: (+49) 64212862148. E-mail: decher@staff.uni-marburg.de.

ORCID

Wendy González: 0000-0002-7535-6883

Author Contributions

W.G. participated in research design; D.R., B.A., and S.R. conducted the experiments; N.D. contributed new reagents or analytic tools; D.R., G.M., S.R., N.D., and W.G. performed data analysis; D.R., F.V.S., N.D., and W.G. wrote or contributed to the writing of the manuscript. All authors have given approval to the final version of the manuscript.

Notes

The authors declare no competing financial interest.

■ ACKNOWLEDGMENTS

The authors thank the Center for Bioinformatics and Molecular Simulations for computational time provided to run molecular docking and molecular dynamics simulations. Authors would like to express their sincere gratitude to Claudia Daza Botero for assistance with manuscript editing. This work was supported by Fondecyt Grant 1140624 to W.G. and a grant of the Deutsche Forschungsgemeinschaft DE1482-4/1 to N.D. CECs is supported by Conicyt's Base Finance Program.

■ ABBREVIATIONS USED

AMS, alanine mutagenesis screening; HRE, halothane response element; K_{2P}, two-pore domain potassium channel; TASK, tandem of pore domains in a weak inwardly rectifying K⁺ channel [TWIK]-related acid-sensitive K⁺ channel; MDs, molecular dynamics simulation(s); MM-GBSA, the molecular mechanics-generalized Born surface area method; POPC, phosphatidyl oleoylphosphatidylcholine; RMSD, root-mean-square deviation; RMSF, root-mean-square fluctuation; SASA, solvent accessible surface area; T1trCC, TASK-1 from TREK-2 in closed–closed fenestration state; T1twiOO, TASK-1 from TWIK-1 in open–open fenestration state; T1trCO, TASK-1 from TRAAK in open–closed fenestration state; T1trOO, TASK-1 from TRAAK in open–open fenestration state

■ REFERENCES

- (1) Goldstein, S.; Bockenhauer, D.; O'Kelly, I.; Zilberberg, N. Potassium Leak Channels and the KCNK Family of Two-P-Domain Subunits. *Nat. Rev. Neurosci.* **2001**, *2* (3), 175–184.
- (2) Enyedi, P.; Czirják, G. Molecular Background of Leak K⁺ Currents: Two-Pore Domain Potassium Channels. *Physiol. Rev.* **2010**, *90* (2), 559–605.
- (3) Lotshaw, D. P. Biophysical, Pharmacological, and Functional Characteristics of Cloned and Native Mammalian Two-Pore Domain K⁺ Channels. *Cell Biochem. Biophys.* **2007**, *47* (2), 209–256.
- (4) Talley, E. M.; Lei, Q.; Sirois, J. E.; Bayliss, D. A. TASK-1, a Two-Pore Domain K⁺ Channel, Is Modulated by Multiple Neurotransmitters in Motoneurons. *Neuron* **2000**, *25* (2), 399–410.
- (5) Rajan, S.; Wischmeyer, E.; Xin Liu, G.; Preisig-Müller, R.; Daut, J.; Karschin, A.; Derst, C. TASK-3, a Novel Tandem Pore Domain Acid-Sensitive K⁺ Channel. An Extracellular Histidine as pH Sensor. *J. Biol. Chem.* **2000**, *275* (22), 16650–16657.
- (6) Kim, D.; Gnatenco, C. TASK-5, a New Member of the Tandem-Pore K⁺ Channel Family. *Biochem. Biophys. Res. Commun.* **2001**, *284* (4), 923–930.
- (7) Lesage, F.; Lazdunski, M. Molecular and Functional Properties of Two-Pore-Domain Potassium Channels. *Am. J. Physiol. Renal Physiol.* **2000**, *279*, F793–F801.
- (8) Miller, A.; Long, S. Crystal Structure of the Human Two-Pore Domain Potassium Channel K2P1. *Science (Washington, DC, U. S.)* **2012**, *335* (6067), 432–441.
- (9) Brohawn, S.; del Marmol, J.; MacKinnon, R. Crystal Structure of the Human K2P TRAAK, a Lipid- and Mechano-Sensitive K⁺ Ion Channel. *Science (Washington, DC, U. S.)* **2012**, *335* (6067), 436–441.
- (10) Brohawn, S.; Campbell, E.; MacKinnon, R. Domain-Swapped Chain Connectivity and Gated Membrane Access in a Fab-Mediated Crystal of the Human TRAAK K⁺ Channel. *Proc. Natl. Acad. Sci. U. S. A.* **2013**, *110* (6), 2129–2134.
- (11) Dong, Y.; Pike, A.; Mackenzie, A.; McClenaghan, C.; Aryal, P.; Dong, L.; Grieben, M.; Goubin, S.; Ruda, G. F.; Clausen, M.; Cao, L.; Brennan, P.; Burgess-Brown, N.; Sansom, M.; Tucker, S. K2P Channel Gating Mechanisms Revealed by Structures of TREK-2 and a Complex with Prozac. *Science (Washington, DC, U. S.)* **2015**, *347* (6227), 1256–1259.

- (12) Aryal, P.; Abd-Wahab, F.; Bucci, G.; Sansom, M. S. P.; Tucker, S. J. A Hydrophobic Barrier Deep within the Inner Pore of the TWIK-1 K2P Potassium Channel. *Nat. Commun.* **2014**, *5*, 1–9.
- (13) Brohawn, S.; Campbell, E.; MacKinnon, R. Physical Mechanism for Gating and Mechanosensitivity of the Human TRAAK K⁺ Channel. *Nature* **2014**, *516* (7529), 126–130.
- (14) Lolicato, M.; Riegelhaupt, P. M.; Arrigoni, C.; Clark, K. A.; Minor, D. L. Transmembrane Helix Straightening and Buckling Underlies Activation of Mechanosensitive and Thermosensitive K2P Channels. *Neuron* **2014**, *84*, 1198–1212.
- (15) Niemeyer, M.; Cid, L.; Gonzalez, W.; Sepulveda, F. Gating, Regulation and Structure in K2P K⁺ Channels: In Varietate Concordia? *Mol. Pharmacol.* **2016**, *90* (3), 309–317.
- (16) Piechotta, P.; Rapedius, M.; Stansfeld, P.; Bollepalli, M.; Erhlich, G.; Andres-Enguix, I.; Fritzenschaft, H.; Decher, N.; Sansom, M.; Tucker, S. The Pore Structure and Gating Mechanism of K2P Channels. *EMBO J.* **2011**, *30* (17), 3607–3619.
- (17) Schewe, M.; Nematian-Ardestani, E.; Sun, H.; Musinszki, M.; Cordeiro, S.; Bucci, G.; de Groot, B. L.; Tucker, S. J.; Rapedius, M.; Baukowitz, T. A Non-Canonical Voltage-Sensing Mechanism Controls Gating in K2P K⁺ Channels. *Cell* **2016**, *164* (5), 937–949.
- (18) Bittner, S.; Bobak, N.; Herrmann, A. M.; Göbel, K.; Meuth, P.; Höhn, K. G.; Stenner, M.-P.; Budde, T.; Wiendl, H.; Meuth, S. G. Upregulation of K2P5.1 Potassium Channels in Multiple Sclerosis. *Ann. Neurol.* **2010**, *68* (1), 58–69.
- (19) Meuth, S.; Bittner, S.; Meuth, P.; Simon, O. J.; Budde, T.; Wiendl, H. TWIK-Related Acid-Sensitive K⁺ Channel 1 (TASK1) and TASK3 Critically Influence T Lymphocyte Effector Functions. *J. Biol. Chem.* **2008**, *283* (21), 14559–14570.
- (20) Kindler, C. H.; Yost, S. C.; Gray, A. T. Local Anesthetic Inhibition of Baseline Potassium Channels with Two Pore Domains in Tandem. *Anesthesiology* **1999**, *90* (4), 1092–1102.
- (21) Czirják, G.; Enyedi, P. Zinc and Mercuric Ions Distinguish TREK from the Other Two-Pore Domain K⁺ Channels. *Mol. Pharmacol.* **2006**, *69* (3), 1024–1032.
- (22) Cotten, J. F. TASK-1 (KCNK3) and TASK-3 (KCNK9) Tandem Pore Potassium Channel Antagonists Stimulate Breathing in Isoflurane Anesthetized Rats. *Anesth. Analg.* **2013**, *116* (4), 810–816.
- (23) Bruner, J. K.; Zou, B.; Zhang, H.; Zhang, Y.; Schmidt, K.; Li, M. Identification of Novel Small Molecule Modulators of K2P18.1 Two-Pore Potassium Channel. *Eur. J. Pharmacol.* **2014**, *740*, 603–610.
- (24) Coburn, C. a.; Luo, Y.; Cui, M.; Wang, J.; Soll, R.; Dong, J.; Hu, B.; Lyon, M. a.; Santarelli, V. P.; Kraus, R. L.; Gregan, Y.; Wang, Y.; Fox, S. V.; Binns, J.; Doran, S. M.; Reiss, D. R.; Tannenbaum, P. L.; Gotter, A. L.; Meinke, P. T.; Renger, J. J. Discovery of a Pharmacologically Active Antagonist of the Two-Pore Domain Potassium Channel K2P9.1 (TASK-3). *ChemMedChem* **2012**, *7* (1), 123–133.
- (25) Flaherty, D. P.; Simpson, D. S.; Miller, M.; Maki, B. E.; Zou, B.; Shi, J.; Wu, M.; McManus, O. B.; Aubé, J.; Li, M.; Golden, J. E. Potent and Selective Inhibitors of the TASK-1 Potassium Channel through Chemical Optimization of a Bis-Amide Scaffold. *Bioorg. Med. Chem. Lett.* **2014**, *24* (16), 3968–3973.
- (26) Kiper, A. K.; Rinné, S.; Rolfes, C.; Ramírez, D.; Seeböhm, G.; Netter, M. F.; González, W.; Decher, N. Kv1.5 Blockers Preferentially Inhibit TASK-1 Channels: TASK-1 as a Target against Atrial Fibrillation and Obstructive Sleep Apnea? *Pfluegers Arch.* **2015**, *467* (5), 1081–1090.
- (27) Streit, A. K.; Netter, M. F.; Kempf, F.; Walecki, M.; Rinné, S.; Bollepalli, M. K.; Preisig-Müller, R.; Renigunta, V.; Daut, J.; Baukowitz, T.; Sansom, M.; Stansfeld, P.; Decher, N. A Specific Two-Pore Domain Potassium Channel Blocker Defines the Structure of the TASK-1 Open Pore. *J. Biol. Chem.* **2011**, *286* (16), 13977–13984.
- (28) Chokshi, R. H.; Larsen, A. T.; Bhayana, B.; Cotten, J. F. Breathing Stimulant Compounds Inhibit TASK-3 Potassium Channel Function Likely by Binding at a Common Site in the Channel Pore. *Mol. Pharmacol.* **2015**, *88*, 926–934.
- (29) Abagyan, R.; Totrov, M. Biased Probability Monte Carlo Conformational Searches and Electrostatic Calculations for Peptides and Proteins. *J. Mol. Biol.* **1994**, *235* (3), 983–1002.
- (30) Russell, R. B.; Barton, G. J. Multiple Protein Sequence Alignment from Tertiary Structure Comparison: Assignment of Global and Residue Confidence Levels. *Proteins: Struct., Funct., Genet.* **1992**, *14* (2), 309–323.
- (31) Humphrey, W.; Dalke, A.; Schulten, K. VMD: Visual Molecular Dynamics. *J. Mol. Graphics* **1996**, *14* (1), 33–38.
- (32) Laskowski, R. A.; MacArthur, M. W.; Moss, D. S.; Thornton, J. M. PROCHECK: A Program to Check the Stereochemical Quality of Protein Structures. *J. Appl. Crystallogr.* **1993**, *26* (2), 283–291.
- (33) Schrödinger, L. *Desmond Molecular Dynamics System, Version 3.0; Epik Version 2.2; Glide, Version 5.7; Impact, Version 5.7; LigPrep, Version 2.5; Phase, Version 3.3; Prime, Version 2.3; SiteMap, Version 2.5*; Virtual Screening Workflow: New York, NY, 2011.
- (34) Jorgensen, W. L.; Maxwell, D. S.; Tirado-Rives, J. Development and Testing of the OPLS All-Atom Force Field on Conformational Energetics and Properties of Organic Liquids. *J. Am. Chem. Soc.* **1996**, *118* (45), 11225–11236.
- (35) Kaminski, G. A.; Friesner, R. A.; Tirado-Rives, J.; Jorgensen, W. L. Evaluation and Reparametrization of the OPLS-AA Force Field for Proteins via Comparison with Accurate Quantum Chemical Calculations on Peptides. *J. Phys. Chem. B* **2001**, *105* (28), 6474–6487.
- (36) Bowers, K. J.; Chow, E.; Xu, H.; Dror, R. O.; Eastwood, M. P.; Gregersen, B. A.; Klepeis, J. L.; Kolossvary, I.; Moraes, M. A.; Sacerdoti, F. D. Scalable Algorithms for Molecular Dynamics Simulations on Commodity Clusters. In *SC 2006 Conference, Proceedings of the ACM/IEEE*; 2006; p 43.
- (37) Smart, O.; Neduvilil, J.; Wang, X.; Wallace, B.; Sansom, M. HOLE: A Program for the Analysis of the Pore Dimensions of Ion Channel Structural Models. *J. Mol. Graphics* **1996**, *14* (6), 354–360.
- (38) Dennington, R.; Keith, T.; Millam, J. *GaussView 5.0.8*; Semichem Inc.: Shawnee Mission, KS, 2009.
- (39) Frisch, M.; Trucks, G. W.; Schlegel, H. B.; Scuseria, G. E.; Robb, M. A.; Cheeseman, J. R.; Scalmani, G.; Barone, V.; Mennucci, B.; Petersson, G. A. *Gaussian 09, Revision A.02*; Gaussian, Inc.: Wallingford, CT, 2009.
- (40) Pan, J.-F.; Chua, S.-J.; Huang, W. Conformational Analysis (Ab Initio HF/3-21G*) and Optical Properties of Poly (Thiophene-Phenylene-thiophene) (PTPT). *Chem. Phys. Lett.* **2002**, *363* (1), 18–24.
- (41) Shelke, S. M.; Bhosale, S. H.; Dash, R. C.; Suryawanshi, M. R.; Mahadik, K. R. Exploration of New Scaffolds as Potential MAO-A Inhibitors Using Pharmacophore and 3D-QSAR Based in Silico Screening. *Bioorg. Med. Chem. Lett.* **2011**, *21* (8), 2419–2424.
- (42) Halgren, T. A.; Murphy, R. B.; Friesner, R. A.; Beard, H. S.; Frye, L. L.; Pollard, W. T.; Banks, J. L. Glide: A New Approach for Rapid, Accurate Docking and Scoring. 2. Enrichment Factors in Database Screening. *J. Med. Chem.* **2004**, *47* (7), 1750–1759.
- (43) Totrov, M.; Abagyan, R. Flexible Ligand Docking to Multiple Receptor Conformations: A Practical Alternative. *Curr. Opin. Struct. Biol.* **2008**, *18* (2), 178–184.
- (44) Feixas, F.; Lindert, S.; Sinko, W.; McCammon, A. Exploring the Role of Receptor Flexibility in Structure-Based Drug Discovery. *Biophys. Chem.* **2014**, *186*, 31–45.
- (45) Ramírez, D.; Caballero, J. Is It Reliable to Use Common Molecular Docking Methods for Comparing the Binding Affinities of Enantiomer Pairs for Their Protein Target? *Int. J. Mol. Sci.* **2016**, *17* (4), 525.
- (46) Ramírez, D. Computational Methods Applied to Rational Drug Design. *Open Med. Chem. J.* **2016**, *10*, 7–20.
- (47) Hou, T.; Wang, J.; Li, Y.; Wang, W. Assessing the Performance of the MM/PBSA and MM/GBSA Methods: 1. The Accuracy of Binding Free Energy Calculations Based on Molecular Dynamics Simulations. *J. Chem. Inf. Model.* **2011**, *51* (1), 69–82.
- (48) Greenidge, P. A.; Kramer, C.; Mozziconacci, J.-C.; Wolf, R. M. MM/GBSA Binding Energy Prediction on the PDBbind Data Set:

Successes, Failures, and Directions for Further Improvement. *J. Chem. Inf. Model.* **2013**, *53* (1), 201–209.

(49) Greenidge, P. A.; Kramer, C.; Mozziconacci, J.-C.; Sherman, W. Improving Docking Results via Reranking of Ensembles of Ligand Poses in Multiple X-Ray Protein Conformations with MM-GBSA. *J. Chem. Inf. Model.* **2014**, *54* (10), 2697–2717.

(50) Sgobba, M.; Caporuscio, F.; Anighoro, A.; Portioli, C.; Rastelli, G. Application of a Post-Docking Procedure Based on MM-PBSA and MM-GBSA on Single and Multiple Protein Conformations. *Eur. J. Med. Chem.* **2012**, *58*, 431–440.

(51) Guimarães, C. R. W.; Cardozo, M. MM-GB/SA Rescoring of Docking Poses in Structure-Based Lead Optimization. *J. Chem. Inf. Model.* **2008**, *48* (5), 958–970.

(52) Adasme-Carreño, F.; Muñoz-Gutierrez, C.; Caballero, J.; Alzate-Morales, J. H. Performance of the MM/GBSA Scoring Using a Binding Site Hydrogen Bond Network-Based Frame Selection: The Protein Kinase Case. *Phys. Chem. Chem. Phys.* **2014**, *16* (27), 14047–14058.

(53) Rastelli, G.; Del Rio, A.; Degliesposti, G.; Sgobba, M. Fast and Accurate Predictions of Binding Free Energies Using MM-PBSA and MM-GBSA. *J. Comput. Chem.* **2010**, *31* (4), 797–810.

(54) Hou, T.; Yu, R. Molecular Dynamics and Free Energy Studies on the Wild-Type and Double Mutant HIV-1 Protease Complexed with Amprenavir and Two Amprenavir-Related Inhibitors: Mechanism for Binding and Drug Resistance. *J. Med. Chem.* **2007**, *50* (6), 1177–1188.

(55) Mena-Ulecia, K.; Tiznado, W.; Caballero, J. Study of the Differential Activity of Thrombin Inhibitors Using Docking, QSAR, Molecular Dynamics, and MM-GBSA. *PLoS One* **2015**, *10* (11), e0142774.

(56) Genheden, S.; Ryde, U. The MM/PBSA and MM/GBSA Methods to Estimate Ligand-Binding Affinities. *Expert Opin. Drug Discovery* **2015**, *10* (5), 449–461.

(57) Lorenzen, S.; Zhang, Y. Identification of near-Native Structures by Clustering Protein Docking Conformations. *Proteins: Struct., Funct., Genet.* **2007**, *68* (1), 187–194.

(58) Yang, T.; Wu, J. C.; Yan, C.; Wang, Y.; Luo, R.; Gonzales, M. B.; Dalby, K. N.; Ren, P. Virtual Screening Using Molecular Simulations. *Proteins: Struct., Funct., Genet.* **2011**, *79* (6), 1940–1951.

(59) Shenkin, P. S.; McDonald, D. Q. Cluster Analysis of Molecular Conformations. *J. Comput. Chem.* **1994**, *15* (8), 899–916.

(60) Martyna, G. J.; Tobias, D. J.; Klein, M. L. Constant Pressure Molecular Dynamics Algorithms. *J. Chem. Phys.* **1994**, *101* (5), 4177–4189.

(61) Bottegoni, G.; Cavalli, A.; Recanatini, M. A Comparative Study on the Application of Hierarchical-Agglomerative Clustering Approaches to Organize Outputs of Reiterated Docking Runs. *J. Chem. Inf. Model.* **2006**, *46* (2), 852–862.

(62) Jorgensen, C.; Darré, L.; Oakes, V.; Torella, R.; Pryde, D.; Domene, C. Lateral Fenestrations in K⁺ Channels Explored Using MD Simulations. *Mol. Pharmaceutics* **2016**, *13*, 2263–2273.

(63) Duprat, F.; Lesage, F.; Fink, M.; Reyes, R.; Heurteaux, C.; Lazdunski, M. TASK, a Human Background K⁺ Channel to Sense External pH Variations near Physiological pH. *EMBO J.* **1997**, *16* (17), 5464–5471.